Infrared Physics & Technology 125 (2022) 104271

Contents lists available at ScienceDirect

Infrared Physics and Technology

journal homepage: www.elsevier.com/locate/infrared

Position effect of laser beam waist in quartz-enhanced photoacoustic spectroscopy

Yi Xie [a,1], Yixin Zhang [b,1], Jie Shao [b], Lei Dong [c], Yibiao Zhang [d], Dehua Zhu [a,*], Xiaojing Chen [e,*], Qi Xia [f]

[a] College of Mechanical and Electrical Engineering, Wenzhou University, Wenzhou 325035, China
[b] Institute of Information Optics, Zhejiang Normal University, Jinhua 321004, China
[c] Institute of Laser Spectroscopy, Shanxi University, Taiyuan 030006, China
[d] Zhejiang Jinhua Guangfu Cancer Hospital, Jinhua 321001, China
[e] College of Electrical and Electronic Engineering, Wenzhou University, Wenzhou 325035, China
[f] Wenzhou University of Technology, Wenzhou 325088, China

ARTICLE INFO

Keywords:
Quartz-enhanced photoacoustic spectroscopy
Laser beam waist
In-plane QEPAS
On-beam QEPAS

ABSTRACT

The position effect of laser beam waist with respect to quartz tuning fork (QTF) on the signal of quartz enhanced photoacoustic spectroscopy (QEPAS) was investigated. A laser beam was collimated by a fiber-coupled Grin collimator (FGC) which was assembled to a QEPAS system. The experimental results showed that the maximum signal amplitude occurs at different distances from the FGCs to the QTF. The relationship between the position of the beam waist and the signal amplitude was analyzed. The influence of the beam waist position in the in-plane QEPAS and the on-beam QEPAS is discussed in detail.

1. Introduction

Quartz-enhanced photoacoustic spectroscopy (QEPAS) was first reported in 2002 [1]. As a promising trace gas detection technique, QEPAS gas sensors have been widely used in atmospheric monitoring, industrial pollution and medical diagnosis due to their high sensitivity, compactness and low cost [2,3]. In QEPAS, a quartz tuning fork (QTF) is used to detect acoustic waves instead of a microphone in the conventional photoacoustic spectroscopy (PAS) [4–8]. Compared to microphones, QTFs have a higher resonant frequency, higher Q-factor, smaller size and lower price. Hence, QEPAS sensors have the advantages of ultra-high sensitivity, high external noise immunity, small dimension, and low cost.

The QEPAS signal amplitude S can be expressed as.

$$S \propto \frac{\alpha P Q}{f_0} \tag{1}$$

where α is the absorption coefficient, P is the optical power, Q is the Q-factor of the QTF, and f_0 is the QTF resonance frequency [9]. According to the above expression, a QEPAS sensor can be optimized in four ways to improve the signal amplitude and detection performance: 1) Use a high-power excitation light source to increase the excitation intensity; 2) Apply a laser source whose wavelength covers the strong molecular absorption band to increase the absorption intensity; 3) Use a quartz tuning fork of low resonance frequency to increase the energy accumulation time; 4) Increase the interaction length of light and gas.

In QEPAS, a laser beam passes through the gap between the two prongs of a QTF to produce acoustical signal. At present, the most common method is the perpendicular-plane quartz enhanced photoacoustic spectroscopy (PP-QEPAS), where the laser beam is perpendicular to the QTF plane [10–12]. In the absence of resonators, the excitation distance of the acoustic wave is determined by the thickness T of the QTF prongs (in microns scale), hence the intensity of the piezoelectric signal generated by the QTF is weak. In order to increase the interaction area between the generated acoustic wave and the QTF, Ma Y et al. changed the direction of incidence laser and proposed an optical gas sensing technique based on in-plane quartz enhanced photoacoustic spectroscopy (IP-QEPAS) [13]. They applied a laser from the top of the QTF to produce an acoustic wave which was considered as a line source, and the excitation distance of the acoustic wave was determined by the length L of QTF prongs (in millimeter scale). There is currently little

* Corresponding authors at: Wenzhou University Chashan University Town, Wenzhou, Zhejiang Province, China
E-mail addresses: zhu_556@163.com (D. Zhu), chenxj@wzu.edu.cn (X. Chen).
[1] These authors contributed equally to this manuscript.

https://doi.org/10.1016/j.infrared.2022.104271
Received 1 May 2022; Received in revised form 18 June 2022; Accepted 18 June 2022
Available online 20 June 2022

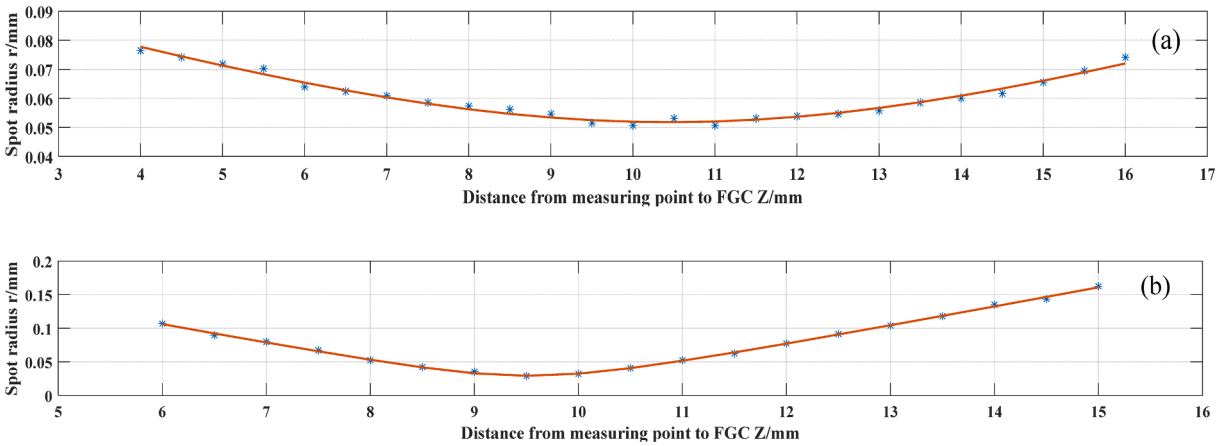

Fig. 1. Fitted curves of the beam radius measurements, (a) The beam waist radius and position of FGC#1 are 0.052 mm and 10.34 mm, respectively. (b) The beam waist radius and position of FGC#2 are 0.029 mm and 9.53 mm, respectively.

literature on IP-QEPAS [14].

In addition, gradient index (Grin) lens is a common micro-optical element which is designed to focus Gaussian beam or serve as a collimator. The Grin lens possesses the advantages of small volume, flat end face and self-focusing property as well as facilitates in coupling with other components. Replacing the block optical collimator and focusing lens with a fiber-coupled Grin collimator (FGC) can significantly reduce the size of the QEPAS system, providing a solution for all-fiber QEPAS spectrophone [15–18].

Previous studies emphasized the position effect of acoustic micro resonator (AmR) with respect to a QTF on the QEPAS signal, and obtained the optimal assembly position of an AmR [19]. However, they did not consider the position effect of the laser beam waist on the QEPAS signal.

In this paper, the position effect of the laser beam waist with respect to a QTF on the signal amplitude of a QEPAS spectrophone was investigated by detecting water vapor in ambient air, at normal atmospheric pressure and room temperature. The optimal assembly position of the FGC has finally been determined. This study is significant for the design and assembly of the QEPAS spectrophones.

2. Experiments

2.1. Beam waist position of incident laser

The radius and position of the beam waist of an incident laser were measured by means of the knife-edge method. A 1.392 μm CW-DFB, fiber-coupled diode laser (NEL, NLK1E5GAAA) was employed as the light source. And the highly collimated laser beam was produced by FGCs. The measurement accuracy is set to one thousandth of a millimeter. As shown in Fig. 1, the radius and position of the beam waist from FGC#1 (OZ Optics, LPF-05–1550-9) were measured to be 0.052 mm and 10.34 mm, respectively. Similarly, those from FGC#2 (OZ Optics, LPF-05–2000-7) were 0.029 mm and 9.53 mm, respectively. The radius of the beam waist from FGC#2 was smaller, but the divergence angle is larger. Therefore, when the interval distance Z was beyond the range of 4.36–14.7 mm, the beam will be partially blocked due to the fact that the beam diameter exceeded the gap (0.3 mm) of the QTF prongs, which reduced the signal-to-noise ratio (SNR).

2.2. 3D printed acoustic detection module

Compared to the conventional mechanical structure, a 3D printed QEPAS spectrophone is characterized by simple structure and small size. Thus, the combination of the FGC and the 3D printing technology facilitates the installation and operation of QEPAS spectrophones [20,21].

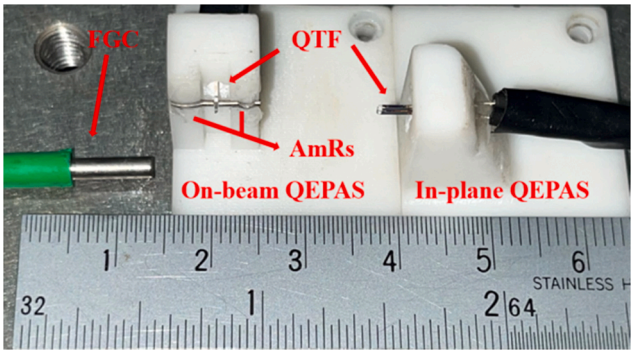

Fig. 2. 3D printed acoustic detection modules for in the in-plane QEPAS and the on-beam QEPAS.

Two 3D printed acoustic detection modules are shown in Fig. 2. Resin (DSM, IMAGE-8000) was used as the material in the 3D print fabrication process, and the QTF and AmRs (inner diameter 0.6 mm, length 4.4 mm) were bonded to the 3D printed part using AB structural glue. In the on-beam QEPAS, the AmRs were placed 0.7 mm down from the top of the QTF (f_0 = 30.460 kHz) prongs, the distance between the AmRs and the QTF plane was about 40 μm [22,23]. In the in-plane QEPAS, the laser beam from the top of the QTF (f_0 = 30.448 kHz) was directed into the center of the prongs.

2.3. Experimental setup

The experimental environment was monitored with a hygrothermograph. The humidity and temperature fluctuated within 1.5% and 2 °C, respectively during the experiment. Wavelength modulated spectroscopy (WMS) and second harmonic (2f) detection technique were used for the sensitive detection of H_2O at 1.392 μm. As shown in Fig. 3, a mixed signal consisted of a 100 mHz triangle wave and a sine wave whose frequency is half of the resonance frequency of QTF was applied to the laser driver (Stanford Research Systems, LDC501) to modulate the laser wavelength. The laser beam which was collimated by the FGC passed through the gap between the two prongs of the QTF. The light-induced sound wave made the two prongs of the QTF vibrate in opposite directions. A 10 MΩ transimpedance amplifier was used to amplify the weak electrical signal generated by the QTF vibration, which was demodulated to a second harmonic signal by a lock-in amplifier (Stanford Research Systems, SR830). A data acquisition card (USB7020) was used to collect the signal.

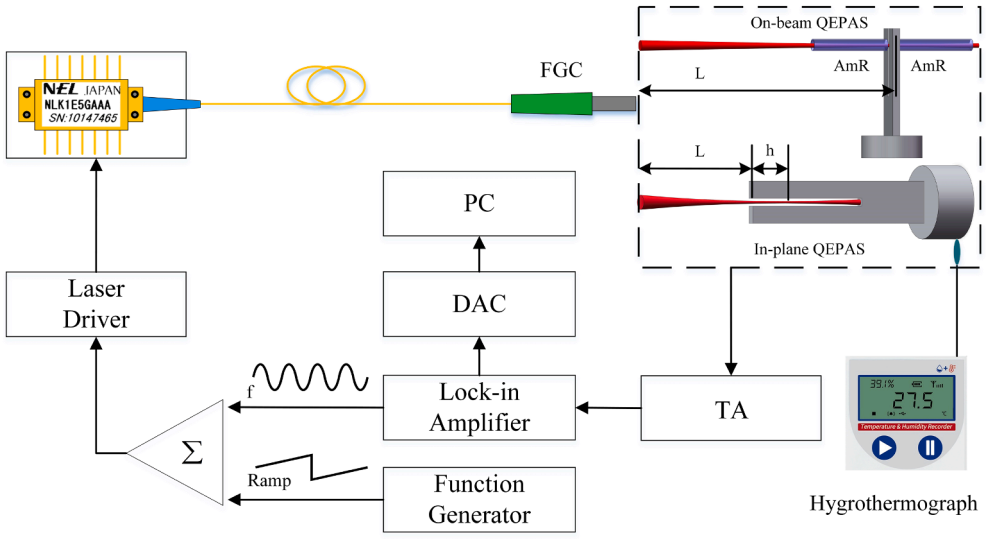

Fig. 3. Schematic configuration of a QEPAS-based sensor platform. TA: transimpedance amplifier. DAC: data acquisition card. PC: Personal Computer. AmR: acoustic micro resonator.

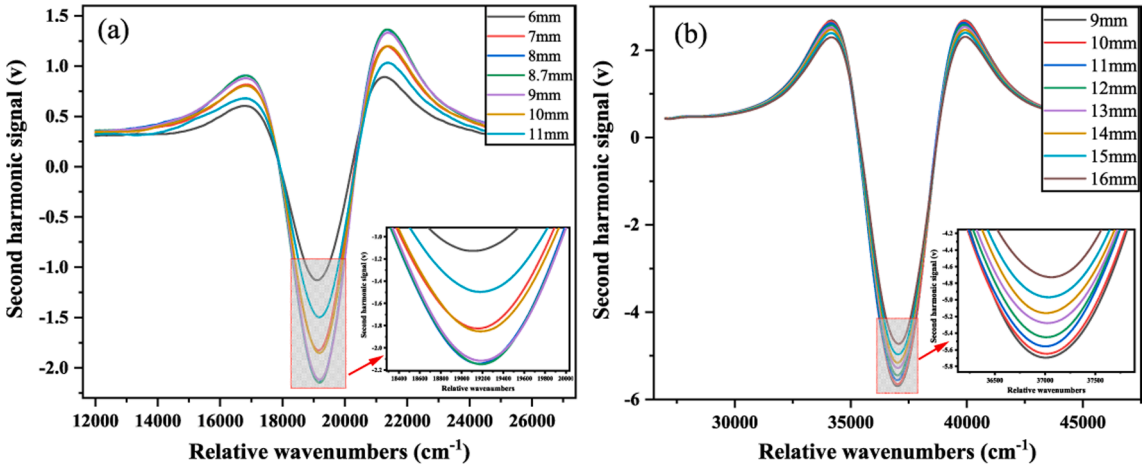

Fig. 4. Second harmonic signals measured with FGC#1 at different positions using (a) the in-plane QEPAS and (b) the on-beam QEPAS.

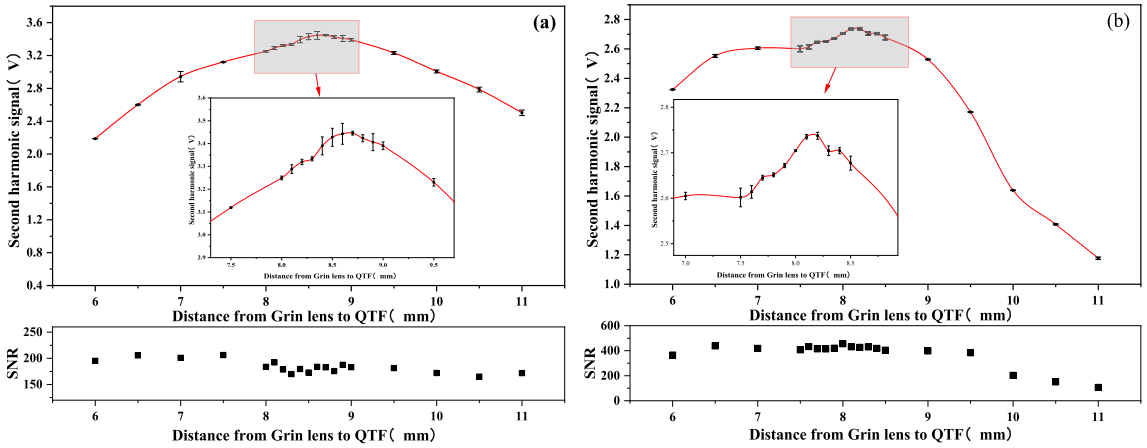

Fig. 5. Signal amplitudes of the in-plane QEPAS as a function of distances from FGCs to the top of the QTF: (a) FGC#1; (b) FGC#2.

3. Results and discussion

FGC#2 with a central wavelength of 2000 nm has a lower transmissivity at 1395 nm than FGC#1 with a central wavelength of 1550 nm. Hence, it resulted in a smaller second harmonic signal. To demonstrate visually the position effect between the FGC and QTF on

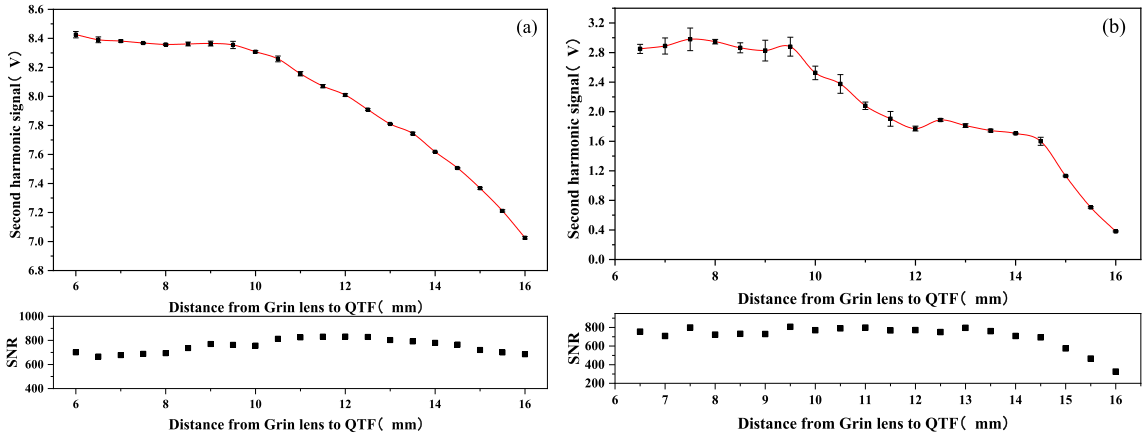

Fig. 6. Signal amplitudes of the on-beam QEPAS as a function of distances from the FGCs to the plane of the QTF: (a) FGC#1; (b) FGC#2.

the signal, Fig. 4 shows the second harmonic signals of the in-plane QEPAS and the on-beam QEPAS when measured at different positions with FGC#1.

We fixed the 3D printed part with the QTF on a 3-axis translation stage with an accuracy of 0.01 mm and adjusted the 3-axis translation stage to gradually move the QTF away from the FGC. The distance L from the FGC to the QTF was measured, and data was collected in the 0.5 mm steps of L. When the acoustic detection module of the in-plane QEPAS was used, several experiments showed that the L value for the maximum signal was always the same. In order to obtain a more accurate L, we collected data in the 0.1 mm steps when approaching the peak. The average value of SNR at each position was recorded. As shown in Fig. 5(a), the distance from FGC#1 to the top of the QTF was 8.7 mm when the signal amplitude reached the maximum. As shown in Fig. 5(b), the distance from FGC#2 to the top of QTF was 8.1 mm when the signal amplitude reached the maximum. It was found that the distances from the different FGCs to the QTF were different at the maximum signal amplitude. Hence, this behavior can be explained by the different beam waist of laser. According to the beam waist positions of FGC#1 and FGC#2, which were 10.34 mm and 9.53 mm, respectively, the beam waist of the laser was all inside the QTF prongs and about h = 1.5 mm away from the top of the QTF. At this moment the vibration amplitude of the QTF prongs was the largest. When FGC#2 was 10 mm away from QTF, the SNR starts dropping since the laser beam diverged and was partially blocked by the QTF prongs.

Similarly, we also compared the results of the on-beam QEPAS acoustic detection module. As shown in Fig. 6(a), the signal amplitude started to drop significantly after the distance from FGC#1 to the QTF exceeded 10.5 mm. While the signal dropped significantly at the distance of 9.5 mm and 14.5 mm for FGC#2 as shown in Fig. 6(b). This behavior was also attributed to the position change of the laser beam waist. It can be found that the maximum signal amplitude was obtained when the distance from the FGCs to the QTF was less than the beam waist position. When L was less than the beam waist position, the closer the FGC to QTF, the higher the laser power, making up for the lower signal, the standing wave inside the AmR was not significantly reduced, so the signal was smooth at this time. However, when FGC#2 was 14.5 mm away from the QTF, the signal amplitude starts dropping since the beam diameter was larger than the gap of the QTF prongs, which resulted in the laser beam partially blocking, and thus reduced the SNR.

4. Conclusions

The position effect of the laser beam waist in QEPAS was studied in this work. At the in-plane QEPAS, the maximum signal amplitude was observed when the laser beam waist was inserted from the top of the QTF to h = 1.5 mm. By using the on-beam QEPAS, the signal amplitude was maximum when the distance from the FGCs to the QTF was smaller than the beam waist position. The beam waist position has a significant effect on signal amplitude, but not on SNR. Furthermore, we found that the QEPAS has high requirements for the incident laser beam, which should not be too divergent and the diameter should not be larger than the gap of QTF prongs. These experiments contribute to the design and assembly of the QEPAS spectrophone and further explores the potential of the in-plane QEPAS to facilitate the integration of AmR with it.

Funding

This study was supported by the National Key R&D Program of China (2019YFE0118200), the Natural Science Foundation of Zhejiang (LY21C200001), the National Natural Science Foundation of China (61775797, 62175137, 62122045), Wenzhou the important item of social and medical development project (ZY2021027), Key Research and Development of Zhejiang Province (2022C03066), Key Science and Technology project of Jinhua City (20213032, 20183026).

Declaration of Competing Interest

The authors declare that they have no known competing financial interests or personal relationships that could have appeared to influence the work reported in this paper.

References

[1] A.A. Kosterev, Y.A. Bakhirkin, R.F. Curl, F.K. Tittel, Quartz-enhanced photoacoustic spectroscopy, OptL. 27 (21) (2002) 1902.
[2] X. Yin, L. Dong, H. Wu, M. Gao, L.e. Zhang, X. Zhang, L. Liu, X. Shao, F.K. Tittel, Compact QEPAS humidity sensor in SF6 buffer gas for high-voltage gas power systems, Photoacoustics 25 (2022) 100319.
[3] Z. Wang, Q. Wang, J.-Y.-L. Ching, J.-C.-Y. Wu, G. Zhang, W. Ren, A portable low-power QEPAS-based CO2 isotope sensor using a fiber-coupled interband cascade laser, Sensors Actuators B: Chem. 246 (2017) 710–715.
[4] B.o. Zhang, K.e. Chen, Y. Chen, B. Yang, M. Guo, H. Deng, F. Ma, F. Zhu, Z. Gong, W. Peng, Q. Yu, High-sensitivity photoacoustic gas detector by employing multi-pass cell and fiber-optic microphone, Opt. Express 28 (5) (2020) 6618–6630.
[5] F. Wang, J. Chang, Q. Zhang, Z. Qin, C. Zhu, Pivotal techniques evaluation in QEPAS system for engineering applications, Measurement 135 (2019) 376–384.
[6] Y.i. Sun, Q. Liu, S. Zha, X. Qiu, H. Chang, S. Feng, G. Guo, X. He, Q. He, C. Li, Sub-ppb nitrogen dioxide detection based on resonant photoacoustic spectroscopy, Microwave Optical Technol. Lett. 63 (8) (2021) 2058–2062.
[7] H. Wu, L. Dong, H. Zheng, Y. Yu, W. Ma, L. Zhang, W. Yin, L. Xiao, S. Jia, F. K. Tittel, Beat frequency quartz-enhanced photoacoustic spectroscopy for fast and calibration-free continuous trace-gas monitoring, Nat. Commun. 8 (1) (2017) 15331.
[8] T. Wei, A. Zifarelli, S. Dello Russo, H. Wu, G. Menduni, P. Patimisco, A. Sampaolo, V. Spagnolo, L. Dong, High and flat spectral responsivity of quartz tuning fork used as infrared photodetector in tunable diode laser spectroscopy, Appl. Phys. Rev. 8 (4) (2021).
[9] P. Patimisco, G. Scamarcio, F.K. Tittel, V. Spagnolo, Quartz-enhanced photoacoustic spectroscopy: a review, Sensors (Basel) 14 (4) (2014) 6165–6206.

[10] Y. Ma, G. Yu, J. Zhang, X. Yu, R. Sun, F.K. Tittel, Quartz enhanced photoacoustic spectroscopy based trace gas sensors using different quartz tuning forks, Sensors (Basel) 15 (4) (2015) 7596–7604.
[11] P. Breitegger, B. Schweighofer, H. Wegleiter, M. Knoll, B. Lang, A. Bergmann, Towards low-cost QEPAS sensors for nitrogen dioxide detection, Photoacoustics 18 (2020) 100169.
[12] H. Lin, Z. Huang, Y. Liu, R. Kan, H. Zheng, R. Zhang, W. Zhu, J. Tang, J. Yu, Z. Chen, F.K. Tittel, Ultra-compact QEPAS acoustic detection module with acoustic wave confinement, Infrared Phys. Technol. 106 (2020).
[13] Y. Ma, S. Qiao, P. Patimisco, A. Sampaolo, Y. Wang, F.K. Tittel, V. Spagnolo, In-plane quartz-enhanced photoacoustic spectroscopy, Appl. Phys. Lett. 116 (6) (2020).
[14] Y. Hong, S. Qiao, Y. Ma, Improved IP-QEPAS sensor based on cylindrical cavity enhancement, Infrared Phys. Technol. 115 (2021).
[15] Y. Ma, Y. Tong, Y. He, X. Jin, F.K. Tittel, Compact and sensitive mid-infrared all-fiber quartz-enhanced photoacoustic spectroscopy sensor for carbon monoxide detection, Opt. Express 27 (6) (2019) 9302–9312.
[16] S. Li, J. Lu, Z. Shang, X. Zeng, Y. Yuan, H. Wu, Y. Pan, A. Sampaolo, P. Patimisco, V. Spagnolo, L. Dong, Compact quartz-enhanced photoacoustic sensor for ppb-level ambient NO2 detection by use of a high-power laser diode and a grooved tuning fork, Photoacoustics 25 (2022).
[17] Z. Li, Z. Wang, Y. Qi, W. Jin, W. Ren, Improved evanescent-wave quartz-enhanced photoacoustic CO sensor using an optical fiber taper, Sensors Actuators B: Chem. 248 (2017) 1023–1028.
[18] W. Feng, Y. Qu, Y. Gao, Y. Ma, Advances in fiber-based quartz enhanced photoacoustic spectroscopy for trace gas sensing, Microwave Opt. Technol. Lett. 63 (8) (2021) 2031–2039.
[19] H. Wu, L. Dong, W. Ren, W. Yin, W. Ma, L. Zhang, S. Jia, F.K. Tittel, Position effects of acoustic micro-resonator in quartz enhanced photoacoustic spectroscopy, Sensors Actuators B: Chem. 206 (2015) 364–370.
[20] X. Yang, Y. Xiao, Y. Ma, Y. He, F. Tittel, A Miniaturized QEPAS trace gas sensor with a 3D-printed acoustic detection module, Sensors (Basel) 17 (8) (2017).
[21] Y. He, Y. Ma, Y. Tong, X. Yu, F.K. Tittel, HCN ppt-level detection based on a QEPAS sensor with amplified laser and a miniaturized 3D-printed photoacoustic detection channel, Opt. Express 26 (8) (2018) 9666–9675.
[22] L. Dong, A.A. Kosterev, D. Thomazy, F.K. Tittel, QEPAS spectrophones: design, optimization, and performance, Appl. Phys. B. 100 (3) (2010) 627–635.
[23] Y. Ma, Y. He, L. Zhang, X. Yu, J. Zhang, R. Sun, F.K. Tittel, Ultra-high sensitive acetylene detection using quartz-enhanced photoacoustic spectroscopy with a fiber amplified diode laser and a 30.72 kHz quartz tuning fork, Appl. Phys. Lett. 110 (3) (2017).